Breast-Dedicated Radionuclide Imaging Systems

David F.C. Hsu[1], David L. Freese[1], and Craig S. Levin[1,2]

[1]Department of Electrical Engineering, Stanford University, Stanford, California; and [2]Departments of Radiology, Bioengineering, and Physics, Stanford University, Stanford, California

Breast-dedicated radionuclide imaging systems show promise for increasing clinical sensitivity for breast cancer while minimizing patient dose and cost. We present several breast-dedicated coincidence-photon and single-photon camera designs that have been described in the literature and examine their intrinsic performance, clinical relevance, and impact. Recent tracer development is mentioned, results from recent clinical tests are summarized, and potential areas for improvement are highlighted.

Key Words: PET; breast; gamma imaging; instrumentation; PEM

J Nucl Med 2016; 57:40S–45S
DOI: 10.2967/jnumed.115.157883

Breast cancer is the most common cancer in women worldwide, with 1.3 million cases diagnosed per year. The current standard of care in breast cancer management has challenges. Physical examinations often find palpable tumors that are already invasive and node-positive. Mammograms are well known for having low specificity and often being inconclusive for patients with dense breasts, leading to unnecessary surgical procedures and patient trauma. The use of noninvasive molecular imaging provides sensitive and specific cellular biologic information to aid in the diagnosis, staging, and treatment evaluation of breast cancer. PET and single-photon emission imaging have shown great diagnostic power in detection of malignant lesions in the body. The conventional systems sitting in the nuclear medicine clinic, however, are general-purpose and have neither the photon sensitivity nor the spatial resolution required to affect earlier stages of breast cancer management. Technologic advances have enabled the creation of high-performance breast-dedicated (BD) radionuclide cameras that show promise for more sensitive cancer detection than standard clinical cameras while also providing better specificity than traditional anatomic imaging modalities such as x-ray mammography. This paper presents novel instrumentation from several different BD system designs that have been studied and evaluates the performance of different BD systems in the clinic.

BD POSITRON EMISSION MAMMOGRAPHY (PEM) AND PET CAMERA DESIGNS

System Configuration

BD PET requires a field of view (FOV) large enough to be clinically relevant for breasts of all sizes, ranging from an average of 11.1–13.7 cm in diameter and 5.7–9.7 cm in length for bra cup sizes A–D (*1*). Detectors are typically arranged in a ring around the breast (annular systems), or in panels on 2 sides (dual-panel systems) or 4 sides (rectangular systems) of the breast. Translatable (*2,3*) and rotatable (*4–7*) detector heads can be used to extend the imaging FOV beyond the detector volume, but to date have had lower sensitivities than stationary systems with equivalent FOVs, and require longer scan times and more complex mechanical designs. For example, the sensitivity of the Shimadzu O-ring system is a factor of 5 higher than that of the Oncovision MAMMI system, which has a similar imaging FOV but uses translating heads (Table 1). Higher photon sensitivity generally allows for shorter scan times to achieve equivalent image quality, as seen with imaging protocols used for stationary (*8*) and translating systems (*9*). Fully tomographic BD PET systems typically involve the patient lying prone with the breasts hanging uncompressed in an annular or rectangular FOV. Better nodal imaging can be accomplished using a C-shaped ring, as fewer lesions lie outside the FOV of the C-ring scanner when compared with the O-ring. However, this design comes at the expense of a significant reduction in photon sensitivity, as shown in Table 1, leading to increased image noise (*8*). Several groups are combining BD PET with CT (*6*) or MRI (*10*), though large-scale clinical studies have yet to be published. Limited-angle tomographic BD PET systems, sometimes referred to as positron emission mammography (PEM) systems, involve mild compression of the breast with a single-axis adjustable FOV. PEM systems are geometrically similar to conventional mammography systems and, using multiple mammographic views of the breast such as craniocaudal or mediolateral oblique, can increase lesion sensitivity beyond that provided by a single view (*3*). However, a major issue caused by the limited angular sampling of the FOV in BD PEM systems is spatial resolution anisotropy, shown in Table 1 (*11*). Dual curved panels can be used to achieve better angular coverage of the breast, leading to higher sensitivity and spatial resolution uniformity (*12*).

Lesions at the chest wall that are missed during imaging plague current BD PET systems (as well as mammography systems). To maximize sensitivity for lesions at the chest wall, the dead area near the chest wall should be minimized (*13*). Dual-panel limited-angle tomography systems that can compress the breast can generally image the chest wall more effectively than ring-based systems, either by taking a different mammographic view of the breast or by bringing into the FOV more of the breast tissue that is near the chest wall. Ring-based tomographic systems will likely continue to be plagued with diagnostic sensitivity issues at the dead area at the chest wall (*14*).

Detector Design Issues

Parallax blurring, caused by uncertainty in the 511-keV photon's depth of interaction (DOI) inside a particular crystal, has a more substantial effect on spatial resolution uniformity in BD PET systems than in conventional whole-body PET scanners because of the increased importance of oblique lines of response (*15*). To

Received Sep. 16, 2015; revision accepted Dec. 29, 2015.
For correspondence or reprints contact: Craig S. Levin, Molecular Imaging and Instrumentation Laboratory, Stanford University, M001 Alway Building, 300 Pasteur Dr., Stanford CA 94040.
E-mail: cslevin@stanford.edu.

TABLE 1
Selected Published BD PET System Specifications and Imaging Performance Statistics

Group	Geometry	FOV (mm)	Crystal type	Crystal size (mm)	Photodetector	Spatial resolution at center of FOV (mm)			DOI resolution	Energy resolution	Timing resolution/ window	Sensitivity (%)
						Radial (*x*)	Tangential (*y*)	Axial (*z*)				
PEMi (*14*)	Annular	110 d, 128 a	LYSO	1.9 × 1.9 × 15	PS PMT	1.58*	1.41	1.31	None	NA	NA/6 ns	6.88%
Shimadzu (*8,41*)	Annular (O)	180 d, 155.5 a (O)	LGSO	1.44 × 1.44 × 4.5	PS PMT	1.6*	1.7	2.0	4.5 mm	16.9% (both)	1.2 ns/NA (both)	16.3% (O)
	C-ring (C)	179 d, 105 a (C)										6.9% (C)
MAMMI (*2,42*)	Annular, translatable	170 d, 170 a‡	LYSO	Monolithic, 40 × 40 × 10	PS PMT	1.6†	1.8	1.9	4 mm	18%	NA/5 ns	3.6%
Texas HOTPET (*43*)	Annular, reconfigurable	540 d, 210 a (breast); 830 d, 130 a (whole body)	BGO	2.68 × 2.68 × 18	PMT	2.7 (breast), 3.3 (whole body) (averaged)*	NA	2.6 (both)	None	NA	NA/15 ns	9.2% (breast); 4.2% (whole body)
Brookhaven PET/MR (*10*)	Annular, multimodal	145.3 d, 96.46 a	LYSO	2.2 × 2.2 × 15	APD	1.2†	1.1	NA	None	NA	NA	NA
Lawrence Berkeley (*16*)	Rectangular	82 *x*, 60 *y*, 50 *z*	LSO	3 × 3 × 30	PMT and SiPD	1.9 mm† (direction unclear)	NA	NA	3.8 mm	24%–51% along crystal	3.4 ns/6 ns	4.94%
West Virginia University PEM/PET (*38*)	Rotating panel, rectangular	150 *x*, 150 *y*, 150 *z*	LYSO	2 × 2 × 15	PS PMT	2.01†	2.04	1.84	None	NA	3.5 ns	6.88%
Clear-PEM (*4,5*)	Rotating panel	162 *x*, 141 *y*	LYSO	2 × 2 × 20	APD	1.4†§ (direction unclear)	NA	1.4	2.5 mm	13%	4 ns	4.3%§
UC Davis PET/CT (*6*)	Rotating panel, multimodal	119 *x*, 119 *y*	LSO	3 × 3 × 20	PS PMT	2.70†	2.73	2.17	None	25%	NA/12 ns	1.64%
M.D. Anderson (*13*)	Dual-panel	200 *x*, 120 *y*	LYSO	1.54 × 1.54 × 10	PMT	1.19*	2.01	4.10	None	17%	NA/7.5 ns	8.9% (avg separation)
PEM I (*19*)	Dual-panel	72 *x*, 72 *y*	BGO	1.9 × 1.9 × 6.5	PS PMT	2.8* (direction unclear)	NA	NA	6.5 mm	53%	12 ns/NA	3%
Pisa (*44*)	Dual-panel	100 *x*, 100 *y*	LYSO	1.9 × 1.9 × 16	PS PMT	NA	NA	NA	None	20%	9.1 ns/NA	NA
Thomas Jefferson Lab (*45*)	Dual-panel	150 *x*, 200 *y*	LGSO	3.03 × 3.03 × 10	PS PMT	4.1 mm (10° acceptance)*	NA	NA	None	NA	NA	0.07% (10°)
						4.7 mm (40° acceptance)	NA	NA				1.35% (40°)
maxPET (*20*)	Dual-panel	150 *x*, 150 *y*	LSO	3 × 3 × 20	PS PMT	2.26 (intrinsic), 4 (imaging)*	NA	NA	None	21.6%	8.1 ns/NA	0.57%
Stanford (*11,46*)	Dual-panel	160 *x*, 100 *y*	LYSO	0.9 × 0.9 × 1	PS APD	0.9 mm†	NA	NA	1 mm	10.6%	15.7 ns/NA	NA
PEM Flex Solo II (*47*)	Dual-panel, translatable	240 *x*, 163 *y*‡	LYSO	2 × 2 × 13	PS PMT	1.94†	1.59	6.45	None	NA	NA/12 ns	0.15% (normalized)
West Virginia University PEM (*7,48*)	Dual-panel or rotating panel	100 *x*, 100 *y*	GSO	3.1 × 3.1 × 10	PS PMT	5.5† (rotating)	5.0 (rotating)	NA (rotating)	None	20%	NA/10 ns	0.016% (3° acceptance)
						3.7 (static)	3.7 (static)	8.9 (static)				0.07% (10° acceptance)
University of Pennsylvania BPET (*12*)	Dual-panel, curved	280 *x*, 210 *y* (active area)	NaI (Tl)	Curved plate detector, 35 × 23 cm surface area	PMT	3.8†	NA	NA	None	10%	NA	0.34% (scanner incomplete)

*Filtered backprojection. †Iterative reconstruction. ‡FOV with translating detector heads. §Simulated.
d = diameter; a = axial; *x*/*y*/*z* = linear orthogonal axes; LYSO = lutetium-yttrium oxyorthosilicate; LGSO = lutetium gadolinium oxyorthosilicate; BGO = bismuth germanate; LSO = lutetium oxyorthosilicate; GSO = germanium oxyorthosilicate; PS = position sensitive; PMT = photomultiplier tube; APD = avalanche photodiode; SiPD = silicon photodiode.

increase diagnostic sensitivity for subcentimeter lesions in the breast, off-center spatial resolution can be improved by incorporating DOI information into the 511-keV photon detectors to reduce the uncertainty of the photon interaction location. DOI can be estimated using the ratio of detected light at opposite sides of a crystal array (*5,16*). Another novel DOI method, shown in Figure 1, is to use thin detector-crystal layers oriented for edge-on photon entry, which allows for both direct DOI measurements and 3-dimensional positioning of intercrystal scatter interactions (*11*). Three-dimensional positioning of multiple photon interactions in the detector gives a measurement of the energy and location of each interaction, which is desirable because a 511-keV photon commonly interacts multiple times in the detector. This 3-dimensional information can be used for recovering 511-keV photon events that would normally be discarded, potentially leading to significant increases in photon sensitivity (*17*). Lastly, DOI can be estimated from crystal arrays that have been engineered to provide depth-dependent scintillation light behavior. This can be done by segmenting the crystal block into different depth layers with different reflective coatings (*18*), by applying crystal light-sharing properties using different cutting patterns (*19*), or by looking at the second moment of the light distribution on monolithic crystal detectors (*2*).

For systems that use discrete crystal elements, decreasing the crystal width improves spatial resolution. Figure 2 shows the correlation between crystal size and spatial resolution for the systems presented in Table 1. Smaller crystals increase the complexity and cost of both crystal manufacturing and crystal readout, especially for systems with one-to-one crystal-to-photodetector coupling architectures. Many groups reduce the number of readout channels

required for small crystals by using position-sensitive variants of photodetectors such as photomultiplier tubes or avalanche photodiodes (Table 1). Another option is to use charge multiplexing (e.g., resistive readout) of photodetector arrays. Light-sharing techniques involving specially engineered crystal reflectors enable position encoding using standard photomultiplier tubes (*13*).

Systems with a high crystal-packing fraction and stopping power will be able to capture a large percentage of emitted photons, allowing for reduced scan time and dose. To reduce the dead area and cost, larger crystals can be mapped onto smaller photodetector-active areas with minimal loss in positioning accuracy. Methods to accomplish this include using devices to reflect light from crystals outside the active area into the active area (*13*), using optical fiber bundles (*20*) or tapered light-guides (*14*) to couple light from the crystal arrays onto detectors, or using monolithic crystals with a truncated pyramid structure to minimize the dead space between detector modules (*2*).

BD SINGLE-PHOTON CAMERA DESIGNS

System Configuration

BD single-photon (γ) cameras can be split into 3 categories: SPECT (*21,22*); limited-angle tomography, commonly called breast tomosynthesis (*23*); and projection imaging by compressing the breast between two stationary collimated scintillation detection panels, a technique referred to as breast-specific γ-imaging (BSGI) (*24*) or molecular breast imaging (MBI) (*25*). In contrast to breast imaging performed with PET, imaging using single-photon radiotracers requires the use of a collimator in front of a detector to provide directional information about the incoming photon.

One important consideration in the design of BSGI systems is whether a single panel is sufficient or dual panels should be used. The benefits of a single panel, such as the Dilon 6800, are lower cost and the ability to perform a biopsy of the breast along the axis of compression (*26*). The benefits of dual panels, such as Gamma Medica's LumaGEM, shown in Figure 3, or GE Healthcare's Discovery NM750b, involve higher photon sensitivity and higher achievable spatial resolution using geometric mean algorithms to combine data from each panel for image generation (*27*). All BD SPECT systems being researched have been paired with CT capability to allow for coregistration of both functional and structural images of the breast, enhancing the diagnostic sensitivity beyond either modality alone. These systems are designed to rotate around an uncompressed hanging breast, with the γ-ray detector placed on an axis offset 90° from the CT source-detector axis on the rotation gantry, as shown in Figure 4. Breast tomosynthesis imaging of compressed breasts can be performed by moving the γ-detector head around a compressed breast over a limited angular range (*28*), although the use of variable-angle slant-hole collimators is also being investigated as a higher-photon-sensitivity option (*29*). BD SPECT imaging of hanging uncompressed breasts use collimated detector heads that rotate around the volume of interest to produce a fully tomographic image.

Detector Design Issues

In single-photon imaging systems, any emitted photons that do not pass through a collimator are not recorded, and photon detection sensitivities for these systems are generally a few orders of magnitude lower than coincidence-based cameras, as shown in Table 2. The low sensitivity can lead to high impact from scattered photons on the final image formation. Ongoing research is examining the effect of scatter on quantification of uptake for SPECT/CT systems with nontraditional acquisition trajectories (*30*). Cadmium zinc telluride, which has better energy resolution than NaI (Table 2), is an attractive detector material for scatter rejection in BD single-photon scanners. Sensitivity can also be improved by reducing the collimator hole length, at the cost of degraded spatial resolution, as shown in Table 2. All BSGI/MBI systems presented in Table 2 have different sets of collimators that are separately optimized for spatial resolution and sensitivity, showing the effects of this tradeoff. The LumaGEM MBI system has made use of their higher sensitivity to conduct dose reduction clinical studies (*25*).

The different collimators used in BD single-photon systems are summarized in Table 2. In general, the spatial resolution and photon detection sensitivity of collimator-based systems are generally inversely proportional to each other, depending on the collimators used, and degrade with increased distance from the collimator. Parallel-hole collimators can maximize the sensitivity of the scanner heads, whereas pinhole collimators sacrifice photon detection sensitivity in exchange for a smaller required detector area, using the pinhole minification effect (*21*). Collimators can also be slanted toward the body for better imaging of the chest wall, something that is not possible with BD PET or PEM cameras. However, slanted collimators can degrade spatial resolution through a DOI effect, which can be mitigated using detector materials with higher attenuation coefficients such as cadmium zinc telluride (*29*).

TRACER DEVELOPMENT FOR BD RADIONUCLIDE IMAGING

In PET imaging of breast cancer, the diagnostic sensitivity and specificity in ^{18}F-FDG, a widely used radiotracer targeting glucose metabolism, can be degraded by differing levels of uptake in necrotic and inflammatory tissue and by ductal versus lobular carcinomas. The single-photon imaging radiotracer ^{99m}Tc-sestamibi, commonly used in BD single-photon imaging clinical trials, is known for indirectly targeting cancer cells by imaging the higher mitochondrial density and transmembrane potential of cancer cells. For BD imaging, new radiotracers have been developed to target more specific biologic characteristics of cancerous breast tissue, such as DNA synthesis for cancer cell proliferation, integrins for angiogenesis, estrogen or progesterone-receptor status, and HER2 status (*31*). These tracers have opened many new possibilities in treatment planning and monitoring of breast cancer.

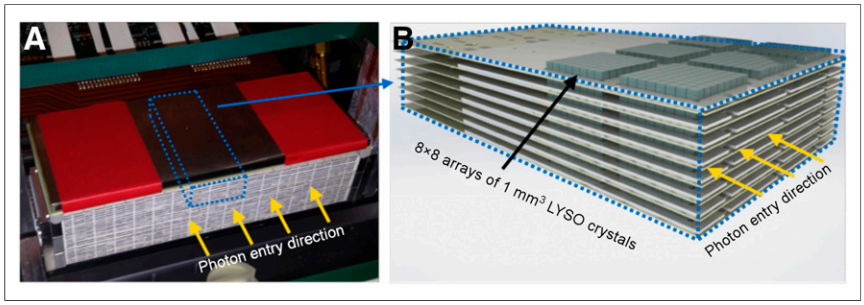

FIGURE 1. Stanford's 1-mm-resolution, 3-dimensional position-sensitive PET scintillation detectors. (A) One panel from actual system, showing edge-on photon entry from imaging FOV. (B) Magnified section depicting edge-on orientation of detectors with respect to incoming photons, allowing for direct measurement of one or more photon DOI locations. LYSO = lutetium-yttrium oxyorthosilicate.

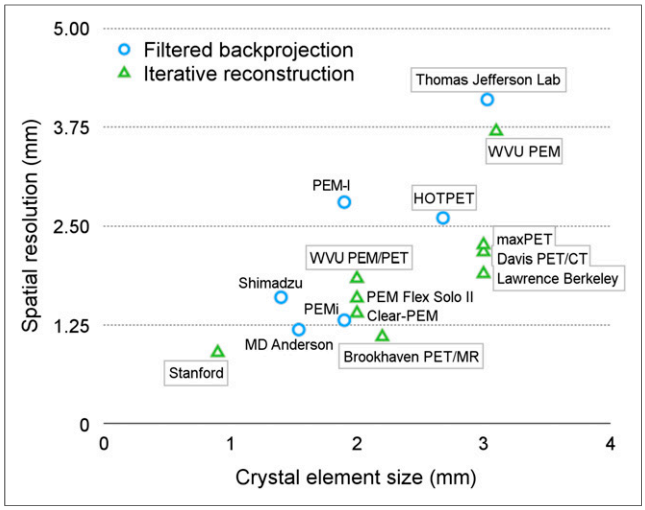

FIGURE 2. Correlation between crystal size and reconstructed spatial resolution along one dimension for breast-dedicated PEM/PET system designs presented in Table 1 that use discrete crystal elements.

CLINICAL TRANSLATION OF BD CAMERAS

In several published studies involving detection of additional tumors in the ipsilateral breast of 388 women with confirmed breast cancer, the Naviscan PEM Flex Solo showed lower sensitivity (51.0% vs. 60.0%) and higher specificity (91.2% vs. 86.3%) than MRI (*32*), higher sensitivity (47% vs. 7%) and lower specificity (91% vs. 96%) than whole-body PET, and higher sensitivity (57% vs. 13%) and lower specificity (91% vs. 95%) than whole-body PET/CT (*33*). In the same group of women, PEM, compared with MRI, showed significantly lower sensitivity (20.0% vs. 93.3%) for cancerous tumors found in the contralateral breast, although it showed higher specificity (95.2% vs. 89.5%) (*34*). Interestingly, some tumors in the central breast are visible on only one of the two mammographic views, an effect that may be caused by anisotropic spatial resolution in PEM systems. Further clinical studies are needed to verify this phenomenon and its clinical diagnostic impact. A recent study with 69 patients, involving the O- and C-shaped scanners developed by Shimadzu, showed significantly lower sensitivity and slightly lower specificity for both scanners than for PET/CT or MRI, caused by lesions lying outside the FOV of the scanners (*8*). These clinical studies, although promising for the development of BD PET and PEM cameras, point to a need to minimize sensitivity loss due to lesions at the chest wall for BD PET devices.

BD PET systems have great potential in breast cancer treatment planning and evaluation, through quantitatively evaluating the SUV of breast lesions during treatment (*35*) and through using high spatial resolution to look at intratumor structures and heterogeneity, which can aid in more accurate biopsy sampling of areas with the highest ^{18}F-FDG uptake (*36*). BD PET systems should have high spatial-resolution uniformity (DOI and full-tomographic sampling) and accurate attenuation correction algorithms, to perform quantitative analysis on tumor uptake. Attenuation correction in the MAMMI BD PET system is performed using PET image segmentation (*2*), whereas the University of California, Davis, BD PET/CT system uses CT image segmentation (*35*). The MAMMI BD PET system is able to accurately quantify breast tumor SUV when compared with conventional PET/CT (*36*) and can examine intratumor structures and heterogeneity (*9*).

BSGI/MBI cameras have had more extensive clinical studies than BD PET or PEM cameras. A study with dual-modality breast tomosynthesis in 17 women found higher sensitivity and specificity than with x-ray tomosynthesis alone (*28*). A meta-analysis on studies involving single-panel BSGI, such as the Dilon 6800, found a combined sensitivity of 95% and specificity of 80% on a total of 2,183 lesions in 8 separate studies (*24*). Dose reduction, one of the biggest challenges for BD radionuclide imaging systems, was examined with dual-panel MBI in a 3-y study of 1,585 women with dense breast parenchyma, using 300-MBq injections of ^{99m}Tc-sestamibi. This injected radiation is a factor of 3–4 lower than conventional BSGI scans and leads to a dose of 2.4 mSv, lower than the annual background radiation level (3 mSv). Combining mammography with MBI increased sensitivity from 24% to 91% and slightly reduced specificity from 89% to 83% (*25*). A cost analysis of this study showed that, even

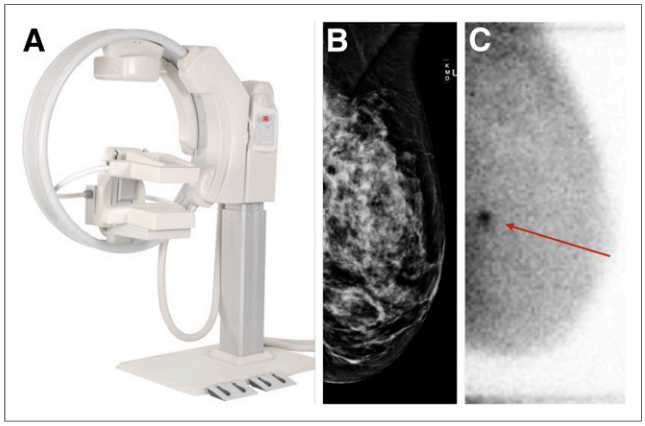

FIGURE 3. (A) Gamma Medica's LumaGEM MBI system. (B) Negative routine digital mammogram interpretation for asymptomatic 55-y-old woman with heterogeneously dense breasts. (C) Referral for MBI secondary screening shows lesion with high uptake. Biopsy showed it to be invasive ductal carcinoma. (Panel A courtesy of Gamma Medica, Inc.; panels B and C courtesy of Dr. Robin Sermis, ProMedica Toledo Hospital.)

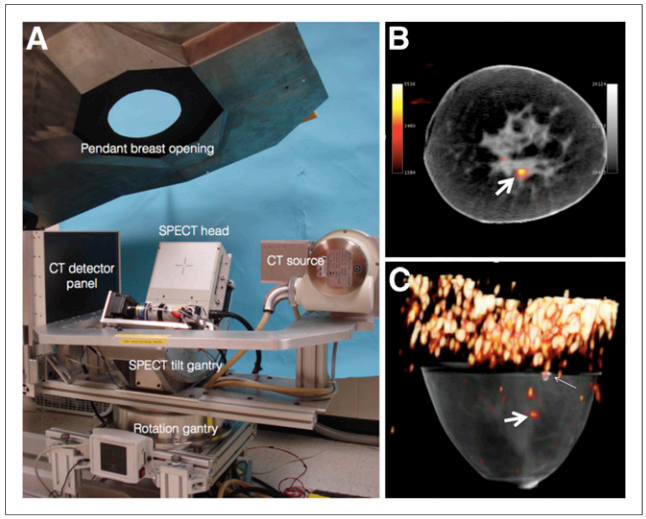

FIGURE 4. (A) Duke's SPECT/CT system. (B) Coronal view (C) and volume rendering of patient scan taken with 790-MBq injection of ^{99m}Tc-sestamibi. Large arrows point to lesion surgically confirmed as ductal carcinoma in situ. Small arrow points to posteriorly located biopsy clip. Myocardial uptake inside chest wall and external scanner fiducial markers outside breast periphery are both visible in C. (Courtesy of Dr. Martin Tornai, Duke Multi-Modality Imaging Lab.)

TABLE 2
Selected Published BD Single-Photon Radionuclide Imaging System Specifications and Imaging Performance Statistics

System	Geometry	FOV (mm)	Patient orientation	Crystal type	Collimator type	Collimator hole diameter/hole length/septal thickness (mm)	Spatial resolution (mm)	Sensitivity (cps/MBq)	Energy resolution at 140 keV
Dilon Diagnostics 6800 (*49*)	Single-panel projection	200 *x*, 200 *y*	Compression	NaI	Parallel-hole	1.22/25/0.15	4.2 (S/C, 3 cm)	31 (EW, 126–154 keV)	9.5%
						1.22/36/0.375	4.0 (S/C, 3 cm)	16 (EW, 126–154 keV)	
Gamma Medica LumaGEM 3200S (*50*)	Dual-panel projection	200 *x*, 160 *y*	Compression	CdZnTe	Parallel-hole	1.22/9.4/0.15	5.6 (S/C, 3 cm)	510 (EW, 110–154 keV)	3.8%
						2.5/25/0.30	4.8 (S/C, 3 cm)	176 (EW, 110–154 keV)	
GE Healthcare Discovery NM750b (*50*)	Dual-panel projection	200 *x*, 200 *y*	Compression	CdZnTe	Parallel-hole	2.1/21/0.40	4.6 (S/C, 3 cm)	318 (EW, 110–154 keV)	6.5%
						2.26/34.7/0.24	4.4 (S/C, 3 cm)	149 (EW, 110–154 keV)	
Duke University SPECT/CT (*22*)	Rotating	200 *x*, 160 *y*	Pendant	CdZnTe	Parallel-hole	1.22/25.4/0.2	3.4 (S/C, 1 cm, planar); 2.7 (S/C, reconstructed at 3-mm rotation radius, sagittal and coronal)	37.9 (EW, 129–151 keV)	6.8%
University of Naples SPECT/CT (*21*)	Rotating	70 *x*, 70 *y*	Pendant	CdTe	Pinhole	1.2-mm effective aperture diameter	5.1 (S/C, 3 cm); 7.2 (S/C, 5 cm)	Not applicable	Not applicable
University of Virginia breast tomosynthesis (*23,51*)	Limited rotation	203 *x*, 152 *y*	Compression	NaI (Tl)	Parallel-hole	1.778/19.99/0.305	3.2 (intrinsic)	147 (EW, 126–154 keV)	17.5%

x/*y* = linear orthogonal axes; EW = energy window; S/C = source-to-collimator distance.

though the addition of MBI to mammography raised the per-patient screening cost from $176 to $571, the increased diagnostic sensitivity of the combination reduced the cost per cancer detected from $55,851 to $47,597 (*37*). The promising reduction in cost per cancer detected, along with the lower dose used in the study, demonstrates the importance to breast cancer diagnostics of a BD radionuclide imaging system with both high diagnostic sensitivity and photon sensitivity.

Biopsy-compatible BD radionuclide imaging cameras can provide molecular guidance for planning a biopsy or for verifying that the correct tissue volumes are sampled by showing the tissue and biopsy needle in real time. This allows the physician to position the needle at the lesion for more accurate sampling of the malignant tissue (*38*). The PEM Flex Solo II uses different attachments to precisely align the biopsy needle with the breast perpendicular to the axis of compression, and alignment scans are taken with a weak line source placed inside the cannula to verify alignment with the lesion, as shown in Figure 5. Noncomparative clinical studies have been conducted to examine the performance of biopsy guidance (*39*). The West Virginia University PEM/PET rectangular system has panels that can swing apart to allow the biopsy arm access to the breast (*38*). Biopsy compatibility in BSGI/MBI systems, because of their 2-dimensional-projection imaging nature, require special collimator designs to find the 3-dimensional position of the lesion without changing the view of the breast. Both the Dilon 6800 (*26*) and the LumaGEM (*40*) use multiple sets of collimators with different directions to achieve this capability and enable accurate estimation of lesion depth.

CONCLUSION

Novel engineering approaches and designs have been summarized for the geometry, detector, and data acquisition systems of BD radionuclide imaging cameras. Clinical trials have shown results that are at least comparable to those of conventional secondary screening methods for breast cancer. However, more work is needed to determine which system design improvements can increase diag-

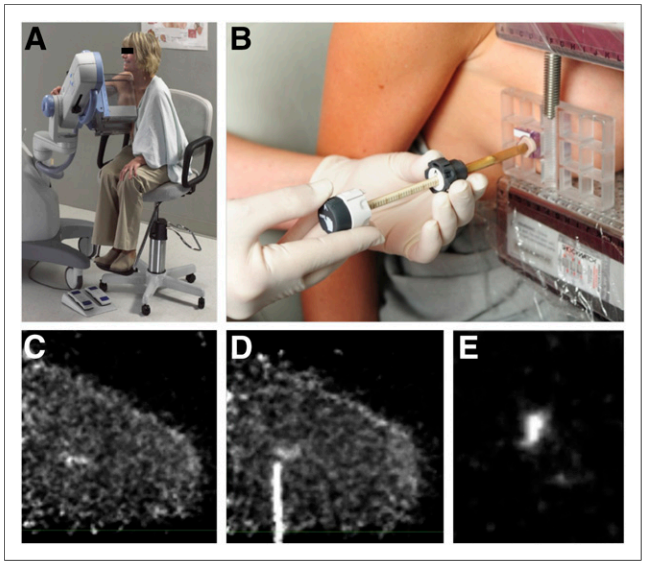

FIGURE 5. (A) Naviscan's PEM Flex Solo II system. (B) Biopsy guidance with attachments to align and guide needle. (C) PEM scan of patient with microinvasive ductal carcinoma in situ. (D) Image of alignment line source and lesion during biopsy. (E) Image of removed sample. (Courtesy of Dr. Kathy Schilling, Boca Raton Regional Hospital.)

nostic sensitivity and specificity and reduce patient dose and the cost of BD radionuclide imaging.

DISCLOSURE

No potential conflict of interest relevant to this article was reported.

REFERENCES

1. Huang SY, Boone JM, Yang K, et al. The characterization of breast anatomical metrics using dedicated breast CT. *Med Phys.* 2011;38:2180–2191.
2. Moliner L, Gonzalez AJ, Soriano A, et al. Design and evaluation of the MAMMI dedicated breast PET. *Med Phys.* 2012;39:5393–5404.
3. MacDonald L, Edwards J, Lewellen T, Haseley D, Rogers J, Kinahan P. Clinical imaging characteristics of the positron emission mammography camera: PEM Flex Solo II. *J Nucl Med.* 2009;50:1666–1675.
4. Abreu MC, Aguiar D, Albuquerque E, et al. Clear-PEM: a PET imaging system dedicated to breast cancer diagnostics. *Nucl Instrum Methods Phys Res A.* 2007;571:81–84.
5. Abreu MC, Aguiar JD, Almeida FG, et al. Design and evaluation of the Clear-PEM scanner for positron emission mammography. *IEEE Trans Nucl Sci.* 2006;53:71–77.
6. Wu Y, Bowen SL, Yang K, et al. PET characteristics of a dedicated breast PET/CT scanner prototype. *Phys Med Biol.* 2009;54:4273–4287.
7. Smith MF, Raylman RR, Majewski S, Weisenberger AG. Positron emission mammography with tomographic acquisition using dual planar detectors: initial evaluations. *Phys Med Biol.* 2004;49:2437–2452.
8. Iima M, Nakamoto Y, Kanao S, et al. Clinical performance of 2 dedicated PET scanners for breast imaging: initial evaluation. *J Nucl Med.* 2012;53:1534–1542.
9. Koolen BB, Vidal-Sicart S, Benlloch Baviera JM, Valdés Olmos RA. Evaluating heterogeneity of primary tumor ^{18}F-FDG uptake in breast cancer with a dedicated breast PET (MAMMI): a feasibility study based on correlation with PET/CT. *Nucl Med Commun.* 2014;35:446–452.
10. Ravindranath B, Junnarkar SS, Purschke ML, et al. Results from prototype II of the BNL simultaneous PET-MR dedicated breast scanner. *IEEE NSS/MIC Record.* 2009;1:3315–3317.
11. Freese DL, Vandenbroucke A, Reynolds PD, et al. Spatial resolution uniformity, isotropy, and the effect of depth of interaction information in a 1mm^3 resolution, limited-angle PET system. *IEEE NSS/MIC Record.* 2014:1–4.
12. Freifelder R, Cardi C, Grigoras I, Saffer JR, Karp JS. First results of a dedicated breast PET imager, BPET, using NaI(Tl) curve plate detectors. *IEEE NSS/MIC Record.* 2001;3:1241–1245.
13. Zhang Y, Ramirez RA, Li H, et al. The system design, engineering architecture, and preliminary results of a lower-cost high-sensitivity high-resolution positron emission mammography camera. *IEEE Trans Nucl Sci.* 2010;57:104–110.
14. Li L, Gu X, Li D, et al. Ability of the positron emission mammography system, PEMi, in detection of millimeter-sized lesions. *IEEE NSS/MIC Record.* 2013:1–7.
15. Lecoq P, Varela J. Clear-PEM, a dedicated PET camera for mammography. *Nucl Instrum Methods Phys Res A.* 2002;486:1–6.
16. Wang GC, Huber JS, Moses WW, Qi J, Choong WS. Characterization of the LBNL PEM camera. *IEEE Trans Nucl Sci.* 2006;53:1129–1135.
17. Levin CS. Promising new photon detection concepts for high-resolution clinical and preclinical PET. *J Nucl Med.* 2012;53:167–170.
18. Tsuda T, Murayama H, Kitamura K, et al. A four-layer depth of interaction detector block for small animal PET. *IEEE Trans Nucl Sci.* 2004;51:2537–2542.
19. Murthy K, Aznar M, Bergman AM, et al. Positron emission mammographic instrument: initial results. *Radiology.* 2000;215:280–285.
20. Doshi NK, Silverman RW, Shao Y, Cherry SR. MaxPET: a dedicated mammary and axillary region PET imaging system for breast cancer. *IEEE Trans Nucl Sci.* 2001;48:811–815.
21. Mettivier G, Russo P, Cesarelli M, et al. Dedicated scanner for laboratory investigations on cone-beam CT/SPECT imaging of the breast. *Nucl Instrum Methods Phys Res A.* 2011;629:350–356.
22. Brzymialkiewicz CN, Tornai MP, Mckinley RL, Bowsher JE. Evaluation of fully 3-D emission mammotomography with a compact cadmium zinc telluride detector. *IEEE Trans Med Imaging.* 2005;24:868–877.
23. Williams MB, More MJ, Narayanan D, et al. Combined structural and functional imaging of the breast. *Technol Cancer Res Treat.* 2002;1:39–42.
24. Sun Y, Wei W, Yang HW, Liu JL. Clinical usefulness of breast-specific gamma imaging as an adjunct modality to mammography for diagnosis of breast cancer: a systemic review and meta-analysis. *Eur J Nucl Med Mol Imaging.* 2013;40:450–463.
25. Rhodes DJ, Hruska CB, Conners AL, et al. Journal club: molecular breast imaging at reduced radiation dose for supplemental screening in mammographically dense breasts. *AJR.* 2015;204:241–251.
26. Kieper DA, Welch BL, Fairchild LH, inventors; Dilon Technologies, Inc., assignee. Gamma guided stereotactic localization system. US Patent US8249693. August 21, 2012.
27. Hruska CB, Phillips SW, Whaley DH, Rhodes DJ, O'Connor MK. Molecular breast imaging: use of a dual-head dedicated gamma camera to detect small breast tumors. *AJR.* 2008;191:1805–1815.
28. Williams MB, Judy PG, Gunn S, Majewski S. Dual-modality breast tomosynthesis. *Radiology.* 2010;255:191–198.
29. Gopan O, Gilland D, Weisenberger A, Kross B, Welch B. Molecular imaging of the breast using a variable-angle slant-hole collimator. *IEEE Trans Nucl Sci.* 2014;53:1143–1152.
30. Mann SD, Tornai MP. Characterization of simulated incident scatter and the impact on quantification in dedicated breast single-photon emission computed tomography. *J Med Imaging.* 2015;2:033504-1–033504-13.
31. Meng Q, Li Z. Molecular imaging probes for diagnosis and therapy evaluation of breast cancer. *Int J Biomed Imaging.* 2013;2013:230487.
32. Berg WA, Madsen KS, Schilling K, et al. Breast cancer: comparative effectiveness of positron emission mammography and MR imaging in presurgical planning for the ipsilateral breast. *Radiology.* 2011;258:59–72.
33. Kalinyak JE, Berg WA, Schilling K, Madsen KS, Narayanan D, Tartar M. Breast cancer detection using high-resolution breast PET compared to whole-body PET or PET/CT. *Eur J Nucl Med Mol Imaging.* 2014;41:260–275.
34. Berg WA, Madsen KS, Schilling K, et al. Comparative effectiveness of positron emission mammography and MRI in the contralateral breast of women with newly diagnosed breast cancer. *AJR.* 2012;198:219–232.
35. Bowen SL, Ferrero A, Badawi RD. Quantification with a dedicated breast PET/CT scanner. *Med Phys.* 2012;39:2694–2707.
36. Koolen BB, Aukema TS, González Martínez AJ, et al. First clinical experience with a dedicated PET for hanging breast molecular imaging. *J Nucl Med Mol Imaging.* 2013;57:92–100.
37. Hruska CB, Conners AL, Jones KN, et al. Diagnostic workup and costs of a single supplemental molecular breast imaging screen of mammographically dense breasts. *AJR.* 2015;204:1345–1353.
38. Raylman RR, Majewski S, Smith MF, et al. The positron emission mammography/tomography breast imaging and biopsy system (PEM/PET): design, construction and phantom-based measurements. *Phys Med Biol.* 2008;53:637–653.
39. Kalinyak JE, Schilling K, Berg WA, et al. PET-guided breast biopsy. *Breast J.* 2011;17:143–151.
40. Weinmann AL, Hruska CB, Conners AL, O'Connor MK. Collimator design for a dedicated molecular breast imaging-guided biopsy system: proof-of-concept. *Med Phys.* 2013;40:012503.
41. Miyake KK, Matsumoto K, Inoue M, et al. Performance evaluation of a new dedicated breast PET scanner using NEMA NU4-2008 Standards. *J Nucl Med.* 2014;55:1198–1203.
42. Soriano A, Sanchez F, Carrilero V, et al. Performance evaluation of the dual ring MAMMI breast PET. *IEEE NSS/MIC Record.* 2013:1–4.
43. Li H, Wong WH, Baghaei H, et al. The engineering and initial results of a transformable low-cost high-resolution PET camera. *IEEE Trans Nucl Sci.* 2007;54:1583–1588.
44. Sportelli G, Belcari N, Guerra P, et al. Reprogrammable acquisition architecture for dedicated positron emission tomography. *IEEE Trans Nucl Sci.* 2011;58:695–702.
45. Turkington TG, Majewski S, Weisenberger AG, et al. A large field of view positron emission mammography imager. *IEEE NSS/MIC Record.* 2002;3:1883–1886.
46. Vandenbroucke A, Reynolds PD, Lau FWY, et al. First measurements of a 512 PSAPD prototype of a sub-mm resolution clinical PET camera. *IEEE NSS/MIC Record.* 2013:1–4.
47. Luo W, Anashkin E, Matthews CG. Performance evaluation of a PEM scanner using the NEMA NU-4 2008 small animal PET standards. *IEEE Trans Nucl Sci.* 2010;57:94–103.
48. Raylman RR, Majewski S, Wojcik R, et al. The potential role of positron emission mammography for detection of breast cancer: a phantom study. *Med Phys.* 2000;27:1943–1954.
49. Williams MB, Williams MB, Goode AR, et al. Performance of a PSPMT based detector for scintimammography. *Phys Med Biol.* 2000;45:781–800.
50. Hruska CB, Weinmann AL, O'Connor MK. Proof of concept for low-dose molecular breast imaging with a dual-head CZT gamma camera. Part I. Evaluation in phantoms. *Med Phys.* 2012;39:3466–3475.
51. Majewski S, Kieper D, Curran C, et al. Optimization of dedicated scintimammography procedure using detector prototypes and compressible phantoms. *IEEE Trans Nucl Sci.* 2001;48:822–829.